Transmission terahertz waveguide-based imaging below the diffraction limit

M. M. Awad and R. A. Cheville[a)]
School of Electrical and Computer Engineering, Oklahoma State University, Stillwater, Oklahoma 74078

(Received 1 December 2004; accepted 5 May 2005; published online 26 May 2005)

Using a terahertz line source from a near dispersion-free parallel plate waveguide, we demonstrate broad bandwidth imaging at terahertz frequencies with subwavelength image resolution. Terahertz radiation is coupled into a parallel plate waveguide with a 100 μm plate spacing, which serves as the imaging aperture. The image data are collected as projections and the final image is reconstructed using the filtered back-projection algorithm, similar to that in x-ray computed tomography. Images taken using a waveguide-based line source demonstrate higher resolution than can be achieved using a confocal cylindrical lens setup. © *2005 American Institute of Physics*. [DOI: 10.1063/1.1942637]

There is currently much interest in developing imaging techniques at terahertz (THz) frequencies. Since the initial demonstration of raster-scanned THz imaging,[1] a wide variety of THz imaging techniques have been demonstrated, including tomographic,[2,3] time reversal,[4] quasioptic,[5] and synthetic aperture methods.[6] While the imaging resolution of all these techniques is limited by the wavelength (submillimeter), near-field imaging techniques using apertures[7] have achieved subwavelength resolution. Such images have great potential, recent imaging techniques using a scanning probe tip have measured features as small as 150 nm.[8]

While THz radiation is severely attenuated upon propagation through subwavelength apertures, this is not the case in propagation through parallel plate waveguides. As shown in recent demonstrations, near dispersion-free propagation of THz pulses occurs in waveguides with losses determined primarily by the overlap of the free space THz field pattern and the waveguide mode.[9] For parallel plate waveguides there is no inherent mode cutoff as the plate spacing decreases, which permits high-brightness line apertures to be created with a plate spacing substantially less than a wavelength. In other words, there is a nearly one-dimensional field distribution at the exit face of the waveguide. We apply the technique of waveguide THz spectroscopy to achieve a subwavelength line excitation, which allows imaging at less than the diffraction limit. This technique has been previously demonstrated at millimeter wave frequencies to achieve spatiotemporal measurements of carrier relaxation.[10,11]

The experimental setup consists of a standard confocal THz time domain spectroscopy system[12] with the THz beam polarized in the *yz* plane, as shown in Fig. 1. The THz beam has a quasi-Gaussian profile with a nominally frequency-independent beam waist (w_1) at the source silicon lens, and a frequency-dependent waist[13] at w_2. Figure 1(a) shows the imaging setup with the two cylindrical lenses and target, placed at the beam waist (w_2). A 0.4 mm thick, 3 in. diameter silicon wafer with a submillimeter planar horn antenna structure is used as the imaging target [see inset in Fig. 2(b)].

To compare waveguide-based imaging to that using confocal optics, two imaging methods were considered. A pair of high-resistivity cylindrical lenses, spaced by the sum of their focal lengths ($f=7.07$ mm), is placed midway between the collimating paraboloidal mirrors, as shown in Fig. 1. The cylindrical lenses create a high-aspect-ratio elliptical focal spot with a frequency-independent beam profile in the *y* direction and frequency-dependent beam profile in the *x* direction. The radius of curvature of the cylindrical lenses is 5 mm, diameter 10 mm, and the height 15 mm. The image plane is situated at the focus of the cylindrical lenses and is parallel to the plane surface of the cylindrical lenses. Second, the same cylindrical lenses were used to couple the collimated THz beam in and out of a parallel plate waveguide.[9] The cylindrical lens-waveguide-cylindrical lens configuration shown in Fig. 1(b) is placed at system beam waist w_2. The cylindrical lenses are spaced one focal length away from the waveguide faces. The exit slit of the waveguide serves as the imaging aperture and is in close proximity ($\sim$25 μm) to the target; that is, the target is placed between the exit slit of the waveguide and the cylindrical lens coupling out of the waveguide, as shown in Fig. 1(b). For both methods, the metallization on the wafer faces the illuminating aperture. The waveguide is fabricated from two optically polished brass slabs with a 400 nm thick gold overcoat on the inside

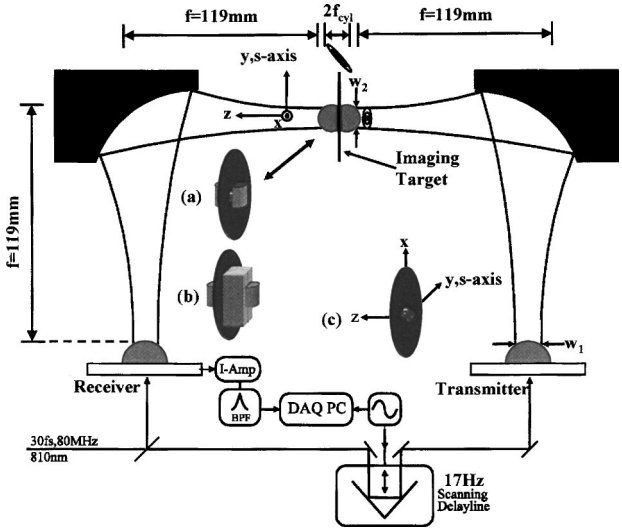

FIG. 1. (a) Cylindrical lens imaging optics with sample. (b) Waveguide imaging aperture with sample. (c) Axis orientation of sample.

[a)]Electronic mail: kridnix@okstate.edu

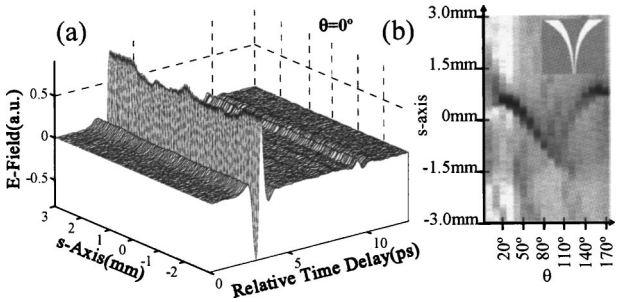

FIG. 2. (a) Time-resolved data for $\theta=0°$, $s=-3$ to 3 mm using waveguide aperture. (b) Waveguide aperture data in radon space with photo of planar horn antenna inset.

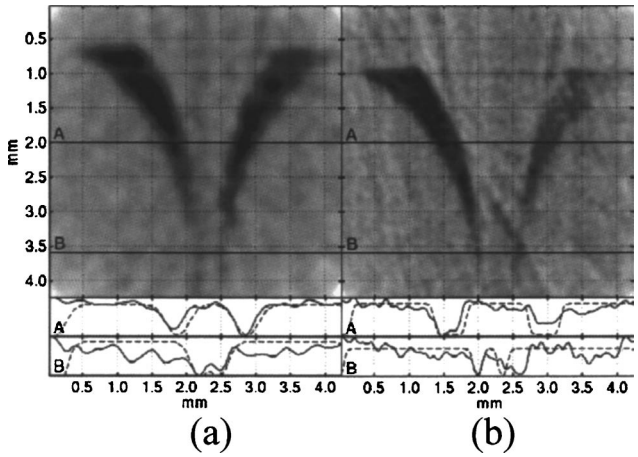

FIG. 3. (a) Cylindrical lens reconstructed image and cross section of image density function at A and B. (b) Waveguide aperture reconstructed image and cross section of image density function at A and B.

waveguide plate walls. The plate spacing is 100 μm, height is 50 mm, and the waveguide length along the direction of propagation is 23 mm. The cylindrical lenses couple THz radiation into a TM_0 (TEM) mode with a frequency-independent mode profile;[9] however, the beam profile in the unguided direction is frequency dependent. Since the waveguide plate spacing is less than a wavelength and because of the broadband nature of the THz pulse, the electric field angular spectrum at the output face of the waveguide will have both propagating and nonpropagating evanescent components.[14] The subwavelength aperture resolution is due to the evanescent waves;[15] however, these evanescent components decay exponentially as the distance from the aperture increases. Therefore, the sample has to be in close contact with the waveguide aperture to achieve subwavelength resolution.

The THz source is a coplanar transmission line fabricated on semi-insulating GaAs and biased at 80 V_{DC}, while the THz detector is a 30 μm dipole antenna fabricated on ion-implanted silicon on sapphire.[16] The THz source and detector are optically gated by a mode-locked Ti:sapphire laser with a 30 fs pulsewidth and a 80 MHz repetition rate at a center wavelength of 810 nm. Time-resolved scans are acquired using a scanning delay line (see Fig. 1).[1] A high-speed, low-noise current amplifier is connected to the THz receiver and converts the detected photocurrent into a voltage. The output from the current amplifier is fed through a bandpass filter to the data acquisition hardware. To improve the signal-to-noise ratio, each projection was averaged over nine iterations.

The object to be imaged is mounted on a rotation stage with an 83 mm clear aperture. The rotation stage is mounted on a motorized translation stage moving in the direction normal to the optical axis. This allows for sample rotation in the xy plane and translation along the y,s axis, as shown in Fig. 1(c). The resolution of rotational and linear motion are 1° and 20 μm, respectively. The rotation stage is aligned such that the optical axis is collinear with the centerline of the rotation stage, where at this position, $s=y=0$ mm. Image projections are acquired by moving the sample across the imaging plane along the y,s direction and rotating the sample once the translation is finished. The images in Fig. 3 were acquired by moving the sample from −3.0 to 3.0 mm along the y axis in 20 μm increments. Since the sample is rotated, and not the aperture, the s axis and y axis coincide. For consistency with notation used in the references, the experiment's y axis corresponds to the s axis in radon space. This measurement was repeated for 18 angles with θ ranging from 0° to 170° in 10° increments. This resulted in 5400 time-resolved scans, each consisting of 600 data points over a time window of 86 ps. Figure 2(a) shows time scans at $\theta=0°$ and sample translation from $s=-3$ mm to $s=3$ mm using the waveguide aperture. The time-resolved data is Fourier transformed and the amplitude of the electric field at 0.6 THz is used to reconstruct the image for both cylindrical lens and waveguide aperture. Figure 2(b) shows the acquired image in (s,θ) space using the waveguide aperture.

Since both the cylindrical lens and the waveguide aperture create high-aspect-ratio illumination, the measured THz signal for any object orientation is a line integral along the imaging aperture:[17]

$$g(s,\theta)=\int_{-\infty}^{\infty} I(\ell,\omega)f(\ell)e^{-\alpha(\ell)\Delta z}d\ell, \tag{1}$$

where $I(\ell,\omega)$ is the frequency-dependent beam profile along the major axis ℓ of the imaging aperture. $f(\ell)$ is the sample pattern along the aperture or the image density function, $\alpha(\ell)$ is the absorption coefficient of the sample along the path of propagation, Δz is the sample thickness, and $d\ell$ is the incremental length along the aperture. For the measured target, the exponential term has values of 0 or 1 due to the high reflectivity of metals and the transparency of the Si substrate at THz frequencies. The measured projections, $g(s,\theta)$, are the radon transform of the image density function $f(x,y)$.[17,18] The radon transform of a function assumes a one-dimensional line source represented by a delta function:[17,18]

$$g(s,\theta)=\int_{-\infty}^{\infty}\int_{-\infty}^{\infty} f(x,y)\,\delta(x\cos\theta+y\sin\theta-s)dxdy. \tag{2}$$

For the THz system, the line source is actually an ellipse where the minor axis is given by the diffraction limited beam waist for the confocal configuration or the waveguide plate spacing for the waveguide aperture. The major axis is frequency dependent, as shown in Fig. 1.

To extract the image from the projection data, the filtered back-projection algorithm is used.[17,18] The resulting image is the original image convolved by the point spread function of the back-projection operator:[17]

$$f_{\text{reconstr}}(x,y) = f(x,y) \otimes (x^2 + y^2)^{-1/2}. \quad (3)$$

The finite waveguide plate spacing or the diffraction limit of the imaging optics results in the reconstructed image being effectively convolved with a two-dimensional Gaussian with the spatial extent of the aperture's spot size along the minor axis. The minimum achievable spot size is determined by the diffraction limit, however, for the strongly curved lens surfaces used here, spherical aberration also affects the spot size.[19,20] The minor axis of the cylindrical lens waist radius is given by $w_{\text{minor}} \cong \lambda f_{\text{cyl}} / \pi w_o(\lambda)$,[21] where the focal length f_{cyl} of the cylindrical lens is 7.07 mm, λ is the free space wavelength, and $w_o(\lambda)$ is the frequency-dependent beam waist at w_2. For the experimental configuration used, the calculated beam diameter along the minor axis of the elliptical focal spots is approximately 300 μm and the beam diameter along the major axis is approximately 15.2 mm at 0.6 THz. The diffraction limit of an imaging system is typically given as $1.22 f\lambda/D$, where f is the focal length of the imaging lens, and $D=10$ mm is the lens aperture. For a frequency of 0.6 THz, the diffraction limit is approximately 430 μm.

Figure 3 shows the reconstructed images at 0.6 THz for both the cylindrical lens setup [Fig. 3(a)] and the waveguide aperture [Fig. 3(b)]. Due to the limited number of projection angles acquired, the reconstructed images exhibit artifacts inherent in the back-projection operation; these can be remedied by acquiring more projection angles.[17] Also shown is a cross section of the image density function taken at lines A and B in Fig. 3 (solid line). The dashed line shows the convolution of the actual target object cross section with a Gaussian corresponding to the minimum focused spot size for the cylindrical lens (300 μm) and the waveguide plate spacing for the waveguide aperture (100 μm). The spreading of the THz beam due to diffraction at the slit aperture of the waveguide is not explicitly accounted for, however, the beam is expected to spread to approximately 112 μm after propagating 25 μm at 0.6 THz.

Comparing cross section A of the reconstructed images in Fig. 3 for both apertures, it can be seen that the transition from Si to metal in Fig. 3(a), as expected, occurs gradually compared to the waveguide aperture image in Fig. 3(b), which shows a much faster transition in the image density function. The metal lines at cross section A, however, are both clearly resolved. At cross section B, on the other hand, the waveguide aperture clearly resolves the 120 μm metallization where the cylindrical lens image can be considered just resolved.

We have demonstrated the use of computed tomography reconstruction techniques in the THz frequency range using two types of imaging apertures. Diffraction limited imaging was achieved using a confocal cylindrical lens aperture. We also demonstrated subdiffraction limit imaging using a parallel plate waveguide as the imaging aperture.

The authors acknowledge the support of the National Science Foundation (NSF9984896), Army Research Office (40992-PH-DPS), and Department of Energy (DE-FG02-02ER45960) for support of this work.

[1] B. B. Hu and M. C. Nuss, Opt. Lett. **20**, 1716 (1995).
[2] D. M. Mittleman, S. Hunsche, L. Boivin, and M. C. Nuss, Opt. Lett. **22**, 904 (1997).
[3] S. Wang, B. Ferguson, D. Abbott, and X. C. Zhang, J. Biol. Phys. **29**, 247 (2003).
[4] A. B. Ruffin, J. Decker, L. Sanchez-Palencia, L. Le Hors, J. F. Whitaker, T. B. Norris, and J. V. Rudd, Opt. Lett. **26**, 681 (2001).
[5] J. O'Hara and D. Grischkowsky, J. Opt. Soc. Am. B **21**, 1178 (2004).
[6] K. McClatchey, M. T. Reiten, and R. A. Cheville, Appl. Phys. Lett. **79**, 4485 (2001).
[7] S. Hunsche, M. Koch, I. Brener, and M. C. Nuss, Opt. Commun. **150**, 22 (1998).
[8] H. T. Chen, R. Kersting, and G. C. Cho, Appl. Phys. Lett. **83**, 3009 (2003).
[9] R. Mendis and D. Grischkowsky, Opt. Lett. **26**, 846 (2001).
[10] J. Bae, T. Okamoto, T. Fujii, K. Mizuno, and T. Nozokido, Appl. Phys. Lett. **71**, 3581 (1997).
[11] T. Nozokido, J. Bae, and K. Mizuno, IEEE Trans. Microwave Theory Tech. **49**, 491 (2001).
[12] M. Vanexter and D. R. Grischkowsky, IEEE Trans. Microwave Theory Tech. **38**, 1684 (1990).
[13] M. Vanexter and D. R. Grischkowsky, IEEE Trans. Microwave Theory Tech. **38**, 1684 (1990).
[14] J. W. Goodman, *Introduction to Fourier Optics*, 2nd ed. (McGraw-Hill, New York, 1996), pp. xviii, 441.
[15] G. A. Massey, Appl. Opt. **23**, 658 (1984).
[16] F. E. Doany, D. Grischkowsky, and C. C. Chi, Appl. Phys. Lett. **50**, 460 (1987).
[17] A. K. Jain, *Fundamentals of digital image processing* (Prentice Hall, Englewood Cliffs, NJ, 1989), pp. xxi, 569.
[18] S. R. Deans, *The Radon Transform and Some of its Applications* (Wiley, New York, 1983), pp. xi, 289.
[19] M. T. Reiten, S. A. Harmon, and R. A. Cheville, J. Opt. Soc. Am. B **20**, 2215 (2003).
[20] M. T. Reiten and R. A. Cheville, Opt. Lett. **30**, 673 (2005).
[21] P. F. Goldsmith and IEEE Microwave Theory and Techniques Society, *Quasioptical Systems: Gaussian Beam Quasioptical Propagation and Applications* (IEEE Press, Piscataway, NJ, 1998), pp. xvii, 412.